Histological evaluation of a chronically-implanted electrocorticographic electrode grid in a non-human primate

You may also be interested in:

Histological evaluation of a chronically-implanted electrocorticographic electrode grid in a non-human primate

Alan D Degenhart[1,2,3,10], James Eles[1,2,10], Richard Dum[2,3],
Jessica L Mischel[1,2], Ivan Smalianchuk[1,2], Bridget Endler[1,2],
Robin C Ashmore[4], Elizabeth C Tyler-Kabara[1,4,5,6],
Nicholas G Hatsopoulos[7,8], Wei Wang[1,2,4,9], Aaron P Batista[1,2,3] and
X Tracy Cui[1,2,6]

[1] Department of Bioengineering, University of Pittsburgh, Pittsburgh, PA, USA
[2] Center for the Neural Basis of Cognition, Pittsburgh, PA, USA
[3] Systems Neuroscience Institute, University of Pittsburgh School of Medicine, Pittsburgh, PA, USA
[4] Department of Physical Medicine and Rehabilitation, University of Pittsburgh, School of Medicine, Pittsburgh, PA, USA
[5] Department of Neurological Surgery, University of Pittsburgh, Pittsburgh, PA, USA
[6] McGowan Institute for Regenerative Medicine, Pittsburgh, PA, USA
[7] Department of Organismal Biology and Anatomy, University of Chicago, Chicago, IL, USA
[8] Committee on Computational Neuroscience, University of Chicago, Chicago, IL, USA
[9] Clinical and Translational Science Institute, University of Pittsburgh, Pittsburgh, PA, USA

E-mail: xic11@pitt.edu, bmewang@gmail.com and apb10@pitt.edu

CrossMark

Abstract

Objective. Electrocorticography (ECoG), used as a neural recording modality for brain-machine interfaces (BMIs), potentially allows for field potentials to be recorded from the surface of the cerebral cortex for long durations without suffering the host-tissue reaction to the extent that it is common with intracortical microelectrodes. Though the stability of signals obtained from chronically implanted ECoG electrodes has begun receiving attention, to date little work has characterized the effects of long-term implantation of ECoG electrodes on underlying cortical tissue. *Approach.* We implanted and recorded from a high-density ECoG electrode grid subdurally over cortical motor areas of a Rhesus macaque for 666 d. *Main results.* Histological analysis revealed minimal damage to the cortex underneath the implant, though the grid itself was encapsulated in collagenous tissue. We observed macrophages and foreign body giant cells at the tissue-array interface, indicative of a stereotypical foreign body response. Despite this encapsulation, cortical modulation during reaching movements was observed more than 18 months post-implantation. *Significance.* These results suggest that ECoG may provide a means by which stable chronic cortical recordings can be obtained with comparatively little tissue damage, facilitating the development of clinically viable BMI systems.

S Online supplementary data available from stacks.iop.org/JNE/13/046019/mmedia

Keywords: brain machine interface, electrocorticography, foreign body response

(Some figures may appear in colour only in the online journal)

[10] Denotes equal contributions.

1. Introduction

Brain-machine interfaces (BMIs) utilize cortical signals to directly control external devices for restoration of motor function in individuals with disabilities (Wolpaw *et al* 2002, Leuthardt *et al* 2006, Schwartz *et al* 2006, Moran 2010). A critical component of a BMI system is the neural recording modality used to extract meaningful information from the brain. The primary modalities used in clinical BMI systems are electroencephalography, electrocorticography (ECoG), local field potentials, and single/multi-unit activity. These methods can be characterized by factors such as performance, decoding stability, longevity, and invasiveness. The choice of a neural recording modality for a particular BMI application must appropriately weigh these factors.

Penetrating intracortical electrode arrays offer the highest spatial and temporal resolution in neural recording. However, the implantation of these arrays disrupts brain tissue and vasculature, and leads to a chronic inflammatory response hallmarked by an aggregation of astrocytes and microglia in a glial scar around the probe, as well as progressive neuronal degeneration at the vicinity of the implanted electrodes (Biran *et al* 2005, Polikov *et al* 2005, McConnell *et al* 2009). This ultimately leads to recorded signal deterioration, manifested as a reduction in the number of electrodes recording individual neurons or a decrease in signal amplitude (Schwartz 2004, Schwartz *et al* 2006, Moran 2010, Chestek *et al* 2011, Freire *et al* 2011, Simeral *et al* 2011, Collinger *et al* 2012, Barrese *et al* 2013). Further, meningeal tissue proliferation and fibrous encapsulation have the potential to dislodge the implanted intracortical devices (Barrese *et al* 2013).

ECoG is a recording modality where electrodes are placed either subdurally (below the dura) or epidurally (on the surface of the dura) to record electrical field potentials generated by aggregate cortical activity. Since ECoG arrays do not penetrate the cortex, they avoid blood–brain barrier disruption and mechanical strain between the stiff electrode and soft neural tissue, which are common for intracortical electrodes. This potentially mitigates some inflammatory burden on the brain. ECoG signals have been found to encode information about arm and hand movements (Leuthardt *et al* 2004, Schalk *et al* 2007, Miller *et al* 2007, Crone *et al* 1998, Pistohl *et al* 2008, Ball *et al* 2009, Kubanek *et al* 2009, Miller *et al* 2009, Wang *et al* 2009, Acharya *et al* 2010, Chao *et al* 2010, Degenhart *et al* 2011a, Shimoda *et al* 2012, Chestek *et al* 2013, Nakanishi *et al* 2013), as well as auditory (Edwards *et al* 2005, Trautner *et al* 2006), visual (Lachaux *et al* 2005), language (Crone *et al* 2001, Mainy *et al* 2007, Kellis *et al* 2010, Pei *et al* 2011, Wang *et al* 2011), and attentional processes (Tallon-Baudry *et al* 2005, Jung *et al* 2008, Ray *et al* 2008). Encouraged by these findings, researchers have begun to investigate ECoG as a potential source of control signals for BMI devices. Human and non-human primate subjects have demonstrated up to three-dimensional control of computer cursors or prosthetic limbs using ECoG (Leuthardt *et al* 2004, Wilson *et al* 2006, Schalk *et al* 2008, Leuthardt *et al* 2011, Schalk and Lethardt 2011, Yanagisawa *et al* 2012, Wang *et al* 2013, Hotson *et al* 2016).

Despite the promise of ECoG in BMI and neuroscience applications, very few studies have evaluated the long-term host-tissue response to either epidural or subdural grids. In humans and non-human primates, subdural and epidural arrays have been implanted for over 1 year with viable neural recording, however these studies did not report end-term tissue health (Morrell and RNS System in Epilepsy Study Group 2011, Shimoda *et al* 2012). Additionally, electrode grids are frequently implanted subdurally for up to 30 d in humans for purposes of epilepsy monitoring. While limited incidents of bleeding, infection, infarction, and functional deficits have been reported in association with these implants, no macroscopic fibrotic growth has been reported in otherwise uncomplicated surgeries (Fountas and Smith 2007, Van Gompel *et al* 2008, Wong *et al* 2009). Some longer-term studies (>1 year) of subdural spinal and cortical stimulators and probes reported encapsulation or dural thickening in the vicinity of the implants (Nashold and Friedman 1972, Pineda 1978, Saitoh *et al* 2000, Sillay *et al* 2013). In rats, just one week after an epidural implantation, connective tissue overgrowth was observed (Schendel *et al* 2013, Schendel *et al* 2014). These studies followed tissue growth around epidural ECoG grids implanted in rats for up to 419 d, showing dural thickening under the arrays and tissue encapsulation over the top of the array as early as one month following implantation (Schendel *et al* 2014). These findings are corroborated by findings of dural thickening at 6 months post subdural implant. Tissue proliferation was correlated with a rise in 1 kHz electrical impedance as early as 1 week, with stabilization at 18 weeks post-implant (Henle *et al* 2011). This would presumably reduce the quality of any neural signal recorded by the ECoG array, though no study has correlated long-term tissue reaction with neural signal quality. While Schendel *et al* and Henle *et al* investigated possible glial reaction to epidural and subdural implantation in the superficial layers of cortex, few studies explore the impact of subdural grids on deeper layers of the cortical tissue, particularly on neuronal health.

The current study explores the host-tissue response to a subdural ECoG grid implanted for 666 d, focusing on both cortical tissue health and fibrosis at the implant site, while also validating device performance by examining neural responses to overt reaching movements. We found that cortical thickness and neuronal density were both unaffected by array implantation. Furthermore, while microglial density was increased in superficial cortical layers, they were in a resting stage morphology, and astrocyte activation was consistent with tissue not under the implant. Finally, though the grid itself was found to be encapsulated in a fibrous envelope upon explantation, we observed robust modulation of ECoG signals in recordings conducted 18 months after implantation.
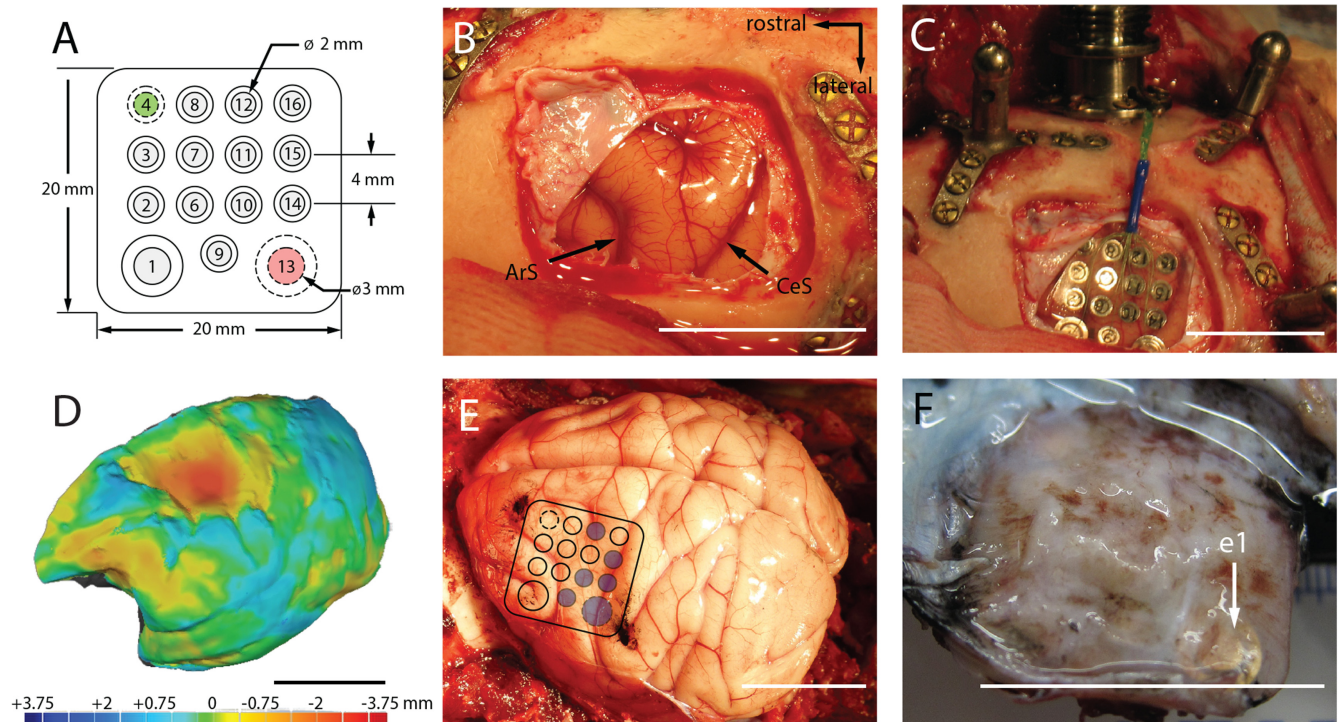
Figure 1. (A). Top view of the electrode grid. The neural recording electrodes (gray) face the cortical surface. The reference (#4, green) and ground (#13, red) electrodes face the dura. (B) Exposure of the left motor cortex prior to implantation (ArS: arcuate sulcus, CeS: central sulcus). (C) Placement of the electrode grid. (D) 3D rendering of the left-hemisphere superimposed on the mirror image of the right-hemisphere. Heat map denotes difference in surface topography between hemispheres in mm. (E) ECoG grid location superimposed on the postmortem brain. Blue circles indicate electrode sites targeted for histological analysis. Black ink marks the observed location of the rostral-medial and caudal-lateral corners of the grid. (F) Underside of the encapsulated grid following explantation. The location of electrode 1 (e1) is indicated by the white arrow. Scale bars in B-F are approximately 2 cm.

2. Methods

All experimental procedures were approved by the Institutional Animal Care and Use Committee of the University of Pittsburgh and were in accordance with the National Institutes of Health's Guidelines for the Care and Use of Laboratory Animals.

2.1. ECoG grid implantation surgery

An adult male Rhesus monkey (*macaca mulatta*) was anesthetized, and a craniotomy was performed to expose the left motor and premotor cortex. The dura was retracted to expose an area approximately 2 × 2 cm between the arcuate and central sulci. A custom-built 15-channel, 1 mm thick silicone ECoG grid with 2 mm diameter platinum electrode sites (figure 1(A), PMT Corp, Chanhassen, MN, USA), identical in construction to FDA-approved electrode grids commonly used for epilepsy monitoring, was placed directly on the exposed brain surface (figures 1(B) to (C)). After positioning, the dura and the bone were reapproximated. Wires from the grid were connected to a Cereport pedestal connector (Blackrock Microsystems, Salt Lake City, UT, USA) affixed to the skull.

2.2. Neural recording and task control

Signals from the ECoG grid were recorded with a g.USBamp Biosignal Amplifier (g.tec Medical Engineering) and sampled at 1200 Hz. All recording, online processing, task control and presentation was performed using the Craniux Brain Computer Interface system (Degenhart *et al* 2011b). Dura-facing electrodes 4 and 13 were used as reference and ground electrodes, respectively, for all recordings (figure 1(A)). Visual stimuli were presented on a 22 inch computer monitor placed approximately 0.8 m from the monkey.

2.3. Hand control task

In order to validate device performance and ECoG signal modulation at long-term time points, we analyzed data recorded approximately 18 months post-implantation (days 542–562 post-implant). During these experiments, the animal performed a standard 2D center-out task in a virtual environment, with the position of the hand controlling the location of a computer cursor in a two-dimensional fronto-parallel plane. The hand position was tracked in real-time using an optical tracking system (Phasespace, San Leandro, CA). Trials began with the appearance of the cursor and central target; the animal was then required to move the cursor to the central target, and hold it there for 400–600 ms. One of eight peripheral targets would then appear, to which the animal was required to reach. A target hold time of 200 ms was enforced. The animal was provided a water reward immediately following successful completion of a trial.

Prior to offline analysis, hand control trials were visually examined for artifacts in both the time and time–frequency domains; all trials exhibiting artifacts during the central hold or target acquisition periods were excluded from further analysis. These artifacts were characterized by large-amplitude, broadband transients across the majority of recording electrodes, and are believed to be the result of jaw movements based on their consistent appearance during the reward period of each trial. Time domain data from the remaining trials were transformed into the time–frequency domain using the Burg autoregressive method (0–200 Hz range, 2 Hz frequency bands, 100th order, 100 ms non-causal window, 33 ms step size), log-transformed, then normalized to pseudo Z-scores relative to the spectral power during the central target hold period. Trials were then manually aligned to movement onset using the cursor speed profile for each trial.

2.4. Explant

Electrodes remained implanted for a total of 666 d, after which the animal was sacrificed and the electrode grid removed. Surgical complications unrelated to the ECoG grid negated the possibility of perfusing the animal before removing the brain. After exposure of the skull, the original bone flap was removed to expose the dura. The skull proximal to the connector, the dura, and the encapsulated electrode grid were then removed as a single piece and the entire brain was extracted. The brain and the encapsulated array were then placed in a 10% formalin + 10% glycerin solution for 8 d followed by 10% formalin + 20% glycerin for 26 d to fixate the tissue. The brain was bisected along the midline and 3D renderings of each hemisphere were generated with a 3D scanner (Faro Platinum Arm, Faro, Warwickshire, UK). Surface topography of the implanted hemisphere was quantitatively compared to the mirror image of the non-implanted hemisphere using Geomagic Studio (Geomagic, Rock Hill, SC). Fixated tissue was then frozen and sectioned into 50 μm sections for staining. Sections were cut perpendicular to the central sulcus. The electrode grid was carefully removed from the encapsulation 'envelope,' which was similarly fixed for 26 d and then stored in phosphate tris azide solution until it was cut into 50 μm sections for staining. Encapsulation tissue was cut perpendicular to the placement of the grid.

2.5. Immunohistochemistry

Cortical sections from implanted and non-implanted hemispheres were mounted on the same slide for comparison, and all slides were processed in the same session to minimize variability. A sample of dura mater distant from the edges of the tissue encapsulation (>2 cm) served as control dura mater for analysis of the encapsulation tissue.

Antibodies for cortical tissue were directed to neurons (NeuN, 1:200, Millipore), astrocytes (GFAP, 1:200, SeroTec), or microglia (Iba-1, 1:500, Fisher); antibodies for encapsulation/dura mater tissue were directed to macrophages (Iba-1, 1:500, Fisher) or fibroblasts/macrophages (Vimentin, 1:250, Millipore). Tissue was first blocked for

30 min in sodium citrate buffer (0.1 M citric acid, 0.1 M sodium citrate, pH 6.0) in room temperature followed by a peroxidase block (10% methanol, 3% hydrogen peroxide) for 20 min in room temperature on a shaker. Then, tissue was blocked in a serum containing blocking buffer (5% normal goat serum, Jackson Labs; 0.1% Triton X-100, Sigma) for 1 h. Tissue was incubated in primary antibody for 12–24 h. Following washes in phosphate buffer saline (PBS), tissue was incubated in 1:250 Alexa Fluor 488 and/or 633 (Invitrogen) for 2 h at room temperature, followed by more PBS washes, 10 min incubation in Hoescht 33342 (1 ul/1 ml; Invitrogen) stain, and more PBS washes. Coverslips were then mounted with Fluoromount-G (Southern-Biotech).

2.6. Confocal imaging

All confocal imaging was performed with an Olympus Fluoview 1000 confocal scanning microscope (Olympus Corporation, Tokyo, Japan). All images were taken with a 20X or 40X objective to optimize cellular resolution and image frame size. Images were taken at multiple focal depths for each frame in order to image the full depth of a tissue slice. This ensured that image analysis was not biased by choice of a single image depth. Confocal laser power, photomultiplier tube voltage (the sensitivity of the image detector), and photomultiplier offset (background level of image detector) were selected to ensure that image pixels did not exceed upper or lower detection limits. Images ($n = 5$ tissue sections per stain) were collected from cortical regions directly under electrode sites in Brodmann Area 4 (specific sites denoted by blue circles in figure 1(E)) on the ECoG array or from the thickest region of both the dorsal and ventral sides of the center of the tissue encapsulation. Images collected were only excluded from analysis on grounds of poor quality of signal, photobleaching, or severe tissue tears during processing. For cortical tissue imaging, images from the contralateral hemisphere were collected for comparison. Images were matched to the same sagittal slice depth and anterior-posterior region of interest as the ipsilateral hemisphere. Tissue encapsulation images were compared to images from random regions of interest of control dura mater retrieved from >2 cm from the tissue encapsulation.

To determine cortical layers and cortical thickness, disconnected images of cortex were stitched to create continuous high-resolution images of the entire cortical depth using Fiji, an Image-J (NIH) plug-in (Preibisch *et al* 2009). Layers I/II-III were discerned from layer V by the location of layer V giant pyramidal cells (Matelli *et al* 1991). Stitched images were used to measure cortical depth ($n = 5$) between conditions. Neuronal and microglial cell densities were determined for layers I/II-III and V with manual counting facilitated by Image J Cell Counter ($n = 5$). Layer I microglia morphology was assessed as previously described (Stence *et al* 2001, Nimmerjahn *et al* 2005, Kozai *et al* 2012). Microglia were deemed to be 'unresponsive' if they were ramified (resting) or activated but not extending processes to the cortical surface, and 'surface directed' if they had activated or ameboid morphology, with processes extended to or along the cortical

surface. Because GFAP labels extensive networks of astrocytic processes, discerning individual cell bodies for cell counting was not possible. Instead, the proportion of cortex occupied by reactive astrocytic signal (% GFAP signal) was determined by first setting a pixel intensity threshold to the mean pixel value of layer I/II-III, where the most intense signal was localized. Because the majority of pixels in a given image are not GFAP-signal, the pixels below the mean can be discounted as noise. Once thresholded, the GFAP signal was determined by automating a count of the non-zero pixels. Implanted cortex and contralateral cortex were compared for all metrics by t-tests with significance level of $\alpha = 0.05$ ($n = 5$ images per group).

We identified cell-types in the encapsulation tissue based on morphology and antibody staining. Vimentin(+)/Iba-1(+) and vimentin($-$)/Iba-1(+) cells were considered to be macrophages if found in the meninges or microglia if found in the parenchyma. Vimentin(+)/Iba-1($-$) cells were considered to be fibroblasts. Multi-nucleated cells were considered cells that contained more than one Hoescht 33342 labeled nuclei in a single cell body. These cells are often found in pathological inflammatory conditions or in the presence of chronically implanted foreign bodies (Brodbeck *et al* 2002, Anderson *et al* 2008, Lynn *et al* 2010).

2.7. Collagen-I imaging

Collagen I, a key component of tissue encapsulation, can be visualized using second- harmonic generation (SHG) imaging. SHG imaging takes advantage of a second-order non-linear optical property of collagen type I to visualize an intrinsically generated optical signal that can be used to locate and quantify collagen I in tissue. This is preferred to traditional histological staining protocols, which have been shown to have less signal specificity and require chemical processing that may alter the tissue quality (Cox *et al* 2003, Strupler *et al* 2007).

SHG images of tissue encapsulation and dura mater were captured using a laser with a Nikon A1Plus multiphoton scanning confocal microscope and Nikon NIS—Elements Microscope Imaging Software. SHG was generated at an 830 nm wavelength, and signal was collected via a bandpass filter that isolated tissue auto-fluorescence (435–700 nm) and a low-pass filter that isolated SHG signal (<492 nm). Images were taken with a 25X objective to maximize signal resolution and imaging frame; stitching software (EIS—Elements Microscope Imaging Software, Nikon) was used to consolidate disconnected images to make a seamless, high-resolution image of the encapsulation through the dorsal-ventral plane.

Encapsulation and dura mater thickness were determined by measuring average thickness of tissue extent as denoted by auto-fluorescence. Because SHG signal was confined within an uninterrupted, fibrous area, percent SHG-signal was measured by dividing the average thickness of SHG area by the total tissue thickness. Such measures were generated for encapsulation tissue from the ventral and dorsal sites, as well as for control dura mater ($n = 5$ tissue sections for all groups). Encapsulation and dura mater thickness and percent SHG signal were compared between ventral encapsulation, dorsal encapsulation, and control dura mater groups by one-way ANOVA tests with Tukey's post-hoc tests. Significance for all comparisons was defined to be $\alpha = 0.05$.

3. Results

3.1. Cortical architecture

Upon sacrifice and explantation, we found that the ECoG grid was fully encapsulated in fibrous tissue that was contiguous with the dura mater (figure 1(F)). The brain underneath the encapsulated ECoG grid was mechanically depressed. We assessed the extent of this depression by generating a 3D rendering of the brain's surface topography. Then, the image of the implanted hemisphere was superimposed onto the non-implanted hemisphere. This allowed us to quantify the topographic differences between the two hemispheres (figure 1(D)). We found that the brain region under the ECoG grid was mechanically depressed by as much as 3.63 mm relative to the same region of the non-implanted hemisphere.

To determine if this gross morphological change resulted in alterations of cortical cytoarchitecture, we evaluated neuronal and glial density as well as cortical thickness under the grid. We compared these metrics of cortical structure to those of the corresponding cortex in the opposite hemisphere (figure 2). The density of neurons labeled with the NeuN antibody in layers I/II-III or layer V was not significantly higher (Student's t-test, $p = 0.5$ and 0.32, respectively) in the cortex under the grid versus the contralateral cortex (figure 2(A)). Similarly, the signal intensity of GFAP antibody labeling of reactive astrocytes in layers I/II-III or layer V was not significantly different between the two hemispheres (figure 2(B); $p = 0.18$ and 0.73, respectively). Only the density of microglia labeled with the Iba-1 antibody and located in the superficial layers (I/II–III) exhibited a significant increase under the array (figure 3(A); t-test $p = 0.027$ for layers I/II-III; 0.24 for layer V). The microglia both under the array and in the contralateral cortex exhibited a qualitatively similar morphology, with only cell density along the dorsal surface of the cortex of either hemisphere (7.6 $\pm$ 1.6 versus 6.6 $\pm$ 1.8 cells mm^{-2} for the implanted and control cortical surface, respectively) showing surface-directed morphology (defined in Methods) (figure 3(B)). These cells typically had processes polarized parallel to the cortical surface. Finally, the thickness of the Nissl-stained cortical tissue under the grid (figure 2(C), top; 2.8 $\pm$ 0.04 mm) was not statistically different from that of the contralateral cortex (figure 2(C), bottom; 2.7 $\pm$ 0.09 mm; t-test: $p = 0.34$). These findings were qualitatively corroborated by observing the transition region of tissue at the edge of the ECoG array and tissue immediately adjacent to the implanted region, where limited changes were observed (supplemental figure A1). Taken together, these tests provide evidence of little to no cytological changes in the cortex underlying the ECoG array.
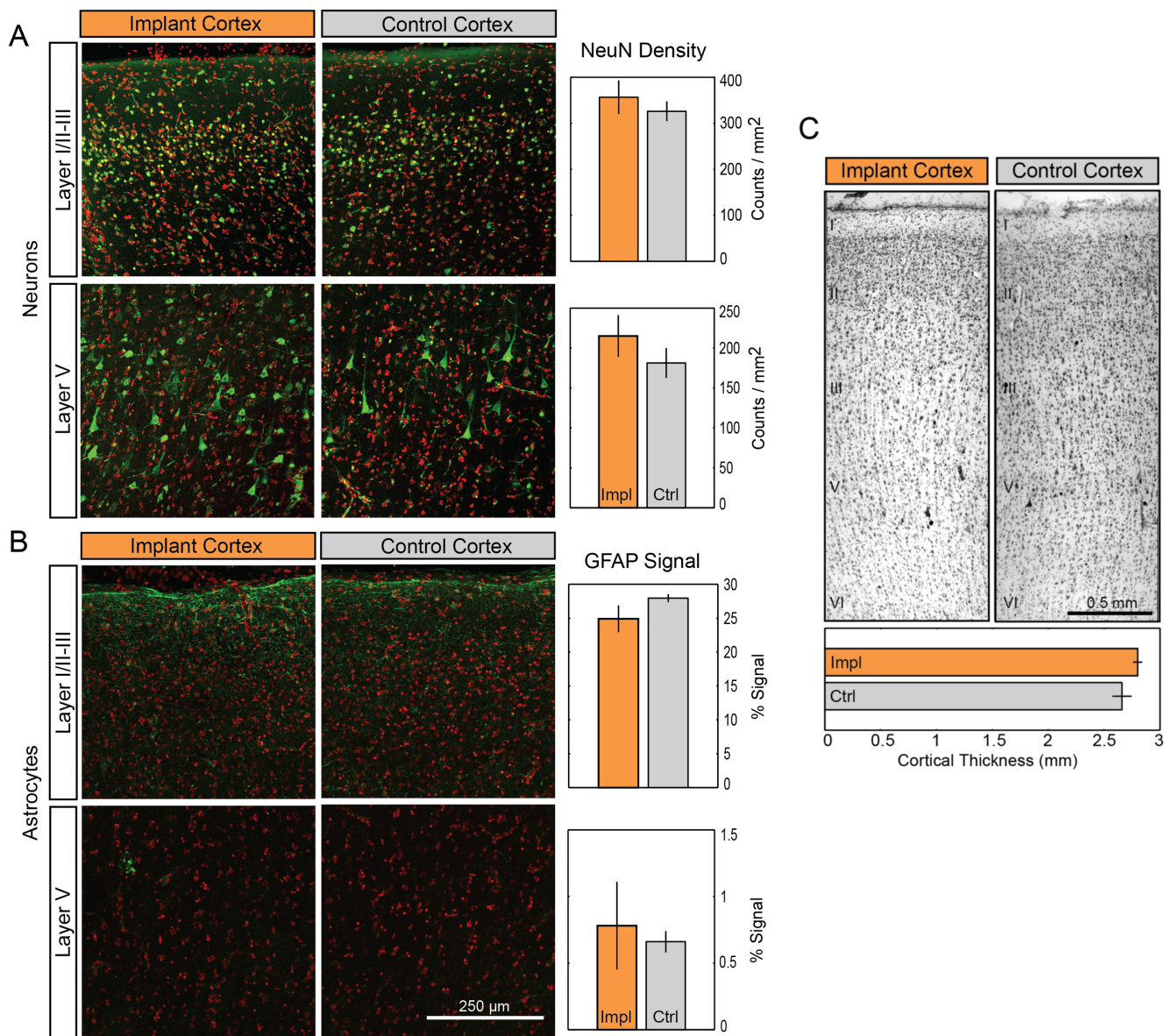
Figure 2. Long-term ECoG grid implantation causes minimal changes in cortical cytoarchitecture. (A) and (B) Neither the density of NeuN-labeled neurons (A; green) nor the signal intensity of GFAP-labeling in astrocytes (B; green) located in layers I/II-III or layer V were significantly affected by implantation. Cell nuclei (red) counterstained with Hoescht 33342. Data presented as mean ± SEM; * denotes significant difference from control (*p* < 0.05). (C) Comparison of Nissl-stained motor cortex between implanted and control hemispheres. Cortical layers are indicated by roman numerals I–VI. *Impl*: implanted cortex. *Ctl*: control cortex.

3.2. Fibrous encapsulation

Chronic subdural ECoG implantation resulted in fibrous encapsulation of the grid. The grid was removed by making an incision along the anterior portion of the encapsulation and pulling the grid with forceps. Surprisingly, the grid offered little mechanical resistance to removal, indicating that adhesion between the grid and encapsulation tissue was minimal. Using SHG imaging, we detected collagen I in sections of both the tissue encapsulation and control dura mater (>2 cm from implantation site). Using filters to image second-harmonic signals and tissue autofluorescence simultaneously, we quantified both the thickness of encapsulation tissue and the percentage of encapsulation tissue that was collagen I-positive (figure 4). Because the dorsal portion of the encapsulation emerged from the original, autografted dura mater, we analyzed it separately from the ventral portion of the encapsulation, which grew *de novo* following initial implantation. Both sides of the tissue encapsulation were compared to control dura mater taken more than 2 cm from the implantation site. There were statistically significant differences in the thicknesses of the tissues (one-way ANOVA: $F(2, 14) = 136.13$, $p < 0.001$), with both dorsal encapsulation (0.82 ± 0.04 mm) and ventral encapsulation (1.76 ± 0.09 mm) being thicker than control dura mater (0.36 ± 0.03 mm; Tukey's post-test: $p = 0.001$). The ventral encapsulation was also significantly thicker than dorsal encapsulation ($p < 0.001$). The encapsulation was
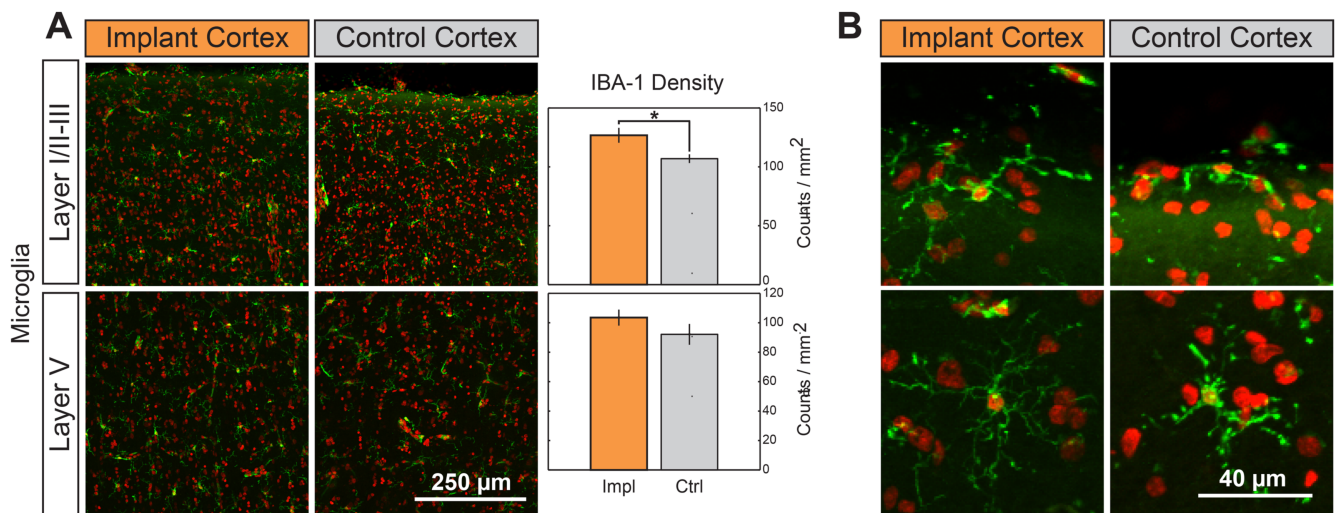
Figure 3. Chronic implantation yields higher microglial density with no change in cell morphology. (A) The density of microglia (green; nuclei in red) was significantly increased in layers I/II-III but not in layer V following implantation. Data presented as mean $\pm$ SEM; [*] denotes significant difference from control ($P < 0.05$). (B) Layer I microglia show no morphological indication of inflammatory response. A small population at the cortical surface of implant and control cortices are polarized along the curvature of the brain, all microglia beneath the surface are unresponsive.

presumably the major contributor to the visible depression of the cortex under the grid.

SHG imaging revealed encapsulation tissue to be comprised of a cellular region that did not express strong SHG signal and a collagenous region that was strongly SHG(+) (figures 4(B) and (E)). Using the tissue thickness derived above, we were able to assess the relative proportions of cellular and collagenous regions by measuring the area of collagenous region (SHG(+) region) and dividing it by tissue thickness. This showed that the proportion of collagenous region was significantly different between the tissues (one-way ANOVA: F $(2, 14) = 44.33$; $p < 0.001$). Control dura mater had a significantly higher percentage of collagenous tissue ($96.4\% \pm 0.33\%$) than either ventral encapsulation ($82.5\% \pm 2.3\%$; Tukey's post-test: $p < 0.01$) or dorsal encapsulation ($58.9\% \pm 4.5\%$; $p < 0.001$). The percentage of collagenous tissue in the ventral encapsulation was also significantly greater than that of the dorsal encapsulation ($p < 0.001$).

In order to determine the cellular composition of the encapsulation we used immunohistochemistry (described in section 2.5). We identified fibroblasts and macrophages in all tissue groups. Control dura mater was largely composed of fibroblasts, many of which exhibited elongated nuclei (figure 5(C)), consistent with previous literature (Adeeb *et al* 2012). Macrophages were sparsely distributed. This resembled the 'collagenous' region (>300 μm from the array; figure 5(B)) of the tissue encapsulation, which also contained elongated fibroblasts and macrophages. The 'cellular' region of encapsulation (<300 μm from the array; figure 5(A)) was highly cell dense with round, mononuclear macrophages as well as multinuclear, foreign body giant cells (vimentin(+-)/Iba-1(+)). We made the mononuclear/multinuclear distinction based on nuclei count (figure 5(A) *inset*). The encapsulation was organized as a gradient, with 'cellular'

tissue closest to the array exhibiting more inflammatory cell activity, and 'collagenous' tissue more distal to the array more closely resembling healthy dura mater.

3.3. Physiological recordings

In order to validate long-term signal modulation, we examined ECoG signals during center-out reaching task trials conducted between days 542 and 562 post-implantation. Signals exhibited clear modulation with target direction (figure 6, supplemental figures B1 and B2). Characteristic decreases in the mu and beta frequency bands (10–30 Hz), in conjunction with increases in the high-gamma band (>60 Hz), were observed. High-gamma band modulation was found to be the strongest over the 70–100 Hz frequency range, and was tightly locked to movement onset. Twelve of the fifteen electrodes exhibited reach-modulated signals. Of the three electrodes not exhibiting reach-related activity, two were the dura-facing reference and ground electrodes and the other an electrically intact electrode that was not recording due to a failure in the cabling connecting the Cereport adapter and neural recording amplifier.

Prior to hand control experiments, a number of recording sessions devoted to BMI control experiments were conducted. However, during post-hoc analysis of these data we discovered that the animal had developed a strategy of using artifacts, possibly the result of jaw movement, to generate directionally-modulated broadband increases in spectral power. We now believe that our earlier report of stable multi-day BMI control was due in part to this strategy (Ashmore *et al* 2012). The presence of these artifacts precludes further analysis of the brain control data, apart from a baseline confirmation of the stability and robustness of the ECoG recordings. We have demonstrated this with representative mean electrode root-mean speed (RMS) amplitude
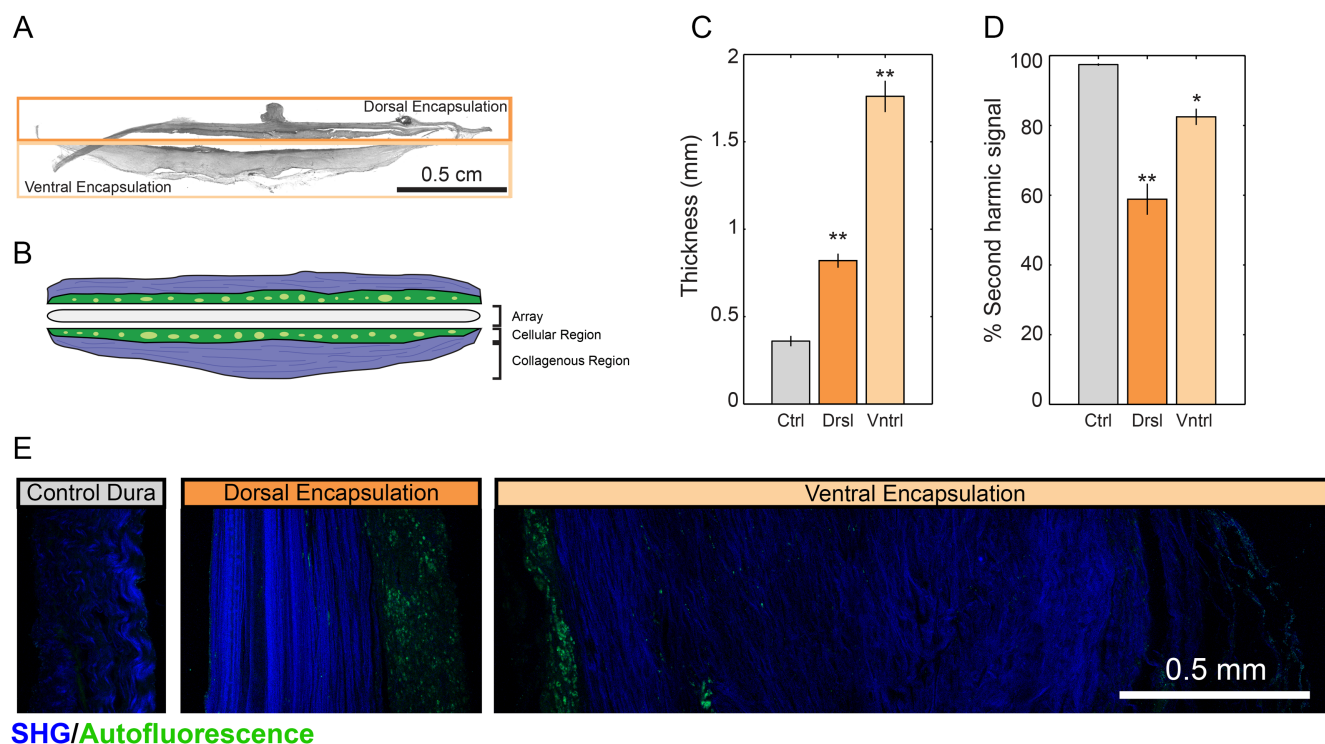
Figure 4. Second-harmonic imaging of fibrous encapsulation reveals fibrous, cell-sparse regions and cell-dense regions in both dorsal and ventral aspects of encapsulation. (A) Sample image of full tissue encapsulation slice. (B) Schematic representation of encapsulation components. (C) Comparison of thickness of dorsal and ventral aspects of encapsulation tissue to control dura. (D) Percentage of SHG(+) tissue was significantly reduced in encapsulation tissue. (E) Sample images of dorsal encapsulation, central encapsulation, and control dura with SHG signal shown in blue and tissue autofluorescence shown in green. Data presented as mean $\pm$ SEM. Asterisks * and ** denote significant differences from control at $p < 0.01$ and $p < 0.001$, respectively.

measurements of ECoG signals, which initially dropped, but stabilized by day 300 post-implant (supplemental figures C1(C) and (D)).

We also tracked mean 20 Hz impedance of all functional electrode sites during some recording sessions from days 52 to 562 post-implant as well as after electrode grid explantation (supplemental section C). Impedance was relatively stable through this time frame, though it fluctuated following surgical interventions (supplemental figure C1(A)). Depending on the impedance measurement method, mean impedance of the grid dropped 6–36 kΩ following removal from the tissue encapsulation (supplemental figure C1(B)).

4. Discussion

4.1. Histological findings

We examined the foreign-body response to a subdural ECoG electrode grid nearly 2 years after implantation. There was fibrotic growth around the electrode grid, resulting in a shallow mechanical depression of the cortex under the array. Despite this, the cellular characteristics of the cerebral cortex underneath the ECoG grid were consistent with that of the tissue of the contralateral hemisphere, where no grid had been placed. Most importantly, cortical thickness and neuronal density of the tissue under the array were statistically indistinguishable from the contralateral tissue, with no

morphological differences apparent at any spatial scale. After accounting for discrepancies in methods, our measurements of thickness and neuronal density for both hemispheres agreed with those of previous anatomical studies of primate frontal cortex (Matelli *et al* 1991, Gittins and Harrison 2004). Noting that cortical thickness and layering was unaffected by the gross mechanical deformation of the brain's surface, it is plausible that the displaced brain was merely pushed into the ventricles, as is observed in cerebral edema and subdural hematoma (Kim and Gean 2011). Only the microglial density of the superficial cortical layers was significantly different between the implanted and non-implanted hemispheres. It is possible that the persistent, unactivated microglia population was part of the foreign body response to the implanted ECoG array, where increased macrophage density persists in the vicinity of the implant for its lifetime (Sanders *et al* 2000, Anderson 2001). It is also conceivable that this activation was not in response to a foreign body, but rather from pervasive mechanical stress caused by the fibrous encapsulation compressing the brain (Ding *et al* 2008, Roth *et al* 2014). With the exception of a population of cells at the cortical surface of both hemispheres, layer I microglia were either ramified or polarized but without processes that extended to the cortical surface, indicating that these microglia were not actively responding to trauma or other noxious stimuli at the surface of the brain (Stence *et al* 2001, Nimmerjahn *et al* 2005, Kozai *et al* 2012, Roth *et al* 2014). The microglia at the surface of
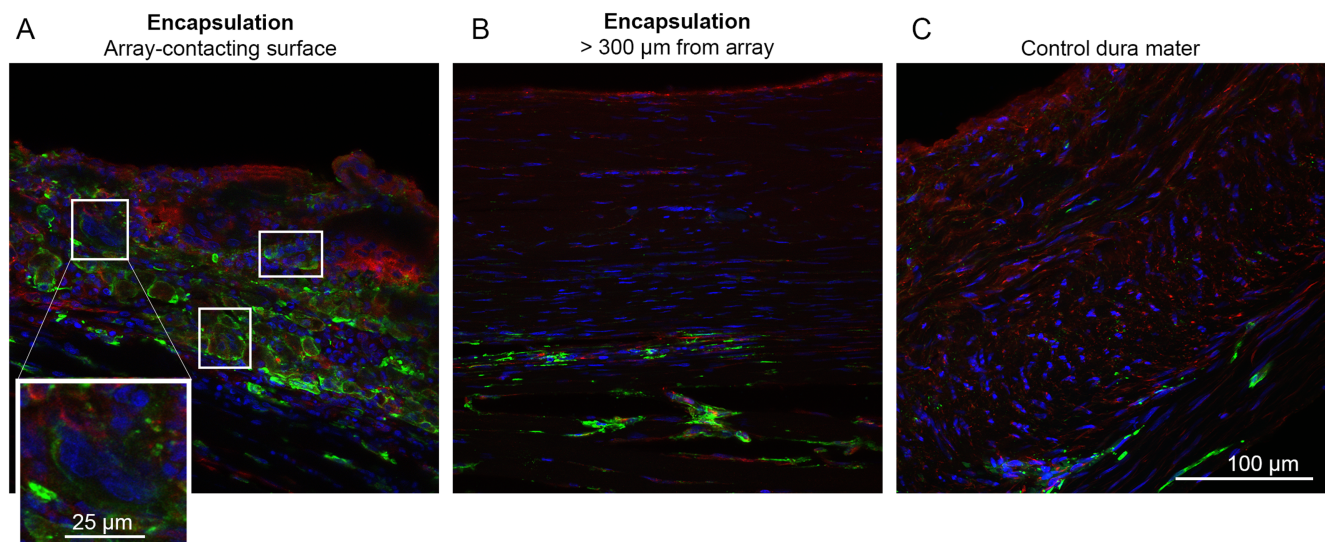
Figure 5. Immunohistochemical staining of encapsulation tissue. Tissue was stained for nuclei (blue; Hoescht 33342) and antibodies directed to macrophages (green; Iba-1) or macrophages/fibroblasts (red; vimentin). (A) Array-contacting aspects of the encapsulation were highly cell dense, populated with macrophages (vimentin(+ or −)/Iba-1(+)) as well as fibroblasts (vimentin(+)/Iba-1(−)). Boxes indicate multi-nucleated giant cells. *Inset*: Magnification of a multinucleated giant cell. (B) Distal portions of encapsulation were hallmarked by elongated fibroblasts and macrophages (vimentin(−)/Iba-1(+)). (C). Control dura mater is largely composed of elongated fibroblasts with infrequent macrophages.

the brain were polarized with processes extending parallel to the cortical surface, similar to a cell type that has been described in healthy mouse cerebellum and rat prefrontal cortex, suggesting the observed cell type is not a result of pathology (Vela *et al* 1995, Konsui *et al* 2014). The astrocytic GFAP expression between control and implanted hemispheres was not different. For both hemispheres, we observed low GFAP expression in the gray matter and relatively strong expression in the glia limitans. This expression pattern has been well documented in healthy macaque brain, with gray matter GFAP expression increasing only in response to trauma or chronic foreign body implantation (Eng *et al* 2000, Peters and Sethares 2002, Griffith and Humphrey 2006). Qualitatively, our finding of low levels of gray-matter GFAP (+) cells under the array suggests that the array was not actively causing trauma to the cortex.

During the grid implantation surgery, we resected the dura mater, replaced it over the ECoG array, and sutured it in place. After the 666 d of implantation, dura mater/fibrous encapsulation tissue was found in a contiguous piece surrounding both the top and bottom of the ECoG grid. Since there were only leptomeninges separating the brain and array at the time of the implant, we assume that the ventral encapsulation grew *de novo* post-implantation. This is similar to recent findings by Schendel *et al* who reported progressive fibrous overgrowth of epidural ECoG grids, with complete encapsulation as early as 1 month post-implantation (Schendel *et al* 2013, Schendel *et al* 2014). The cellular distribution in the dorsal and ventral tissue encapsulation was distinct from dura mater elsewhere in the brain, and implied that the wound-healing response to implantation consisted of a stereotypic foreign body response, which involves aggregation of mononuclear macrophages and multinucleated foreign

body giant cells to the implant site and encapsulation of the device in a collagenous envelope. Aggregated cells and tissue encapsulation generally persist through the lifetime of an implant, with pro-inflammatory cytokine expression diminishing within the first month as anti-inflammatory/pro-wound healing cytokines are expressed (Brodbeck *et al* 2002, Anderson *et al* 2008, Lynn *et al* 2010). The fibrous encapsulation demarcates the final stage of wound healing in which the tissue disrupted by implantation is either regenerated from cells of the original cell type, or replaced with fibrous connective tissue. Given that dura mater is already largely fibrous connective tissue and mesenchymally derived fibroblasts, it was not clear to us the extent to which the tissue encapsulation was fibrous encapsulation or remodeled/regrown dura mater (Anderson 2001, Anderson *et al* 2008, Adeeb *et al* 2012). We observed a gradient where tissue proximal to the implant more closely resembled fibrous encapsulation, and tissue distal to the implant more closely resembled control dura mater.

Both the dorsal encapsulation and ventral encapsulation were thicker than the control dura mater, which would be expected of a foreign body tissue encapsulation. In the case of autografted, dorsal encapsulation, dural thickening may have also been an inevitable consequence of craniotomy and/or durotomy that was simply exacerbated by the presence of a foreign body. This is seen in epidural ECoG implants, where encapsulation with ventral and/or dorsal dural thickening has been reported in long-term implants (Schendel *et al* 2014). Merely performing a craniotomy triggered a 3.8 fold increase in dural thickness at 3 weeks, with a reduction to a 2.6 fold increase at 3 months in New Zealand white rabbits (Nunamaker and Kipke 2010). Replacing dura with an alginate hydrogel resulted in a 2.8 fold increase of dural thickness of
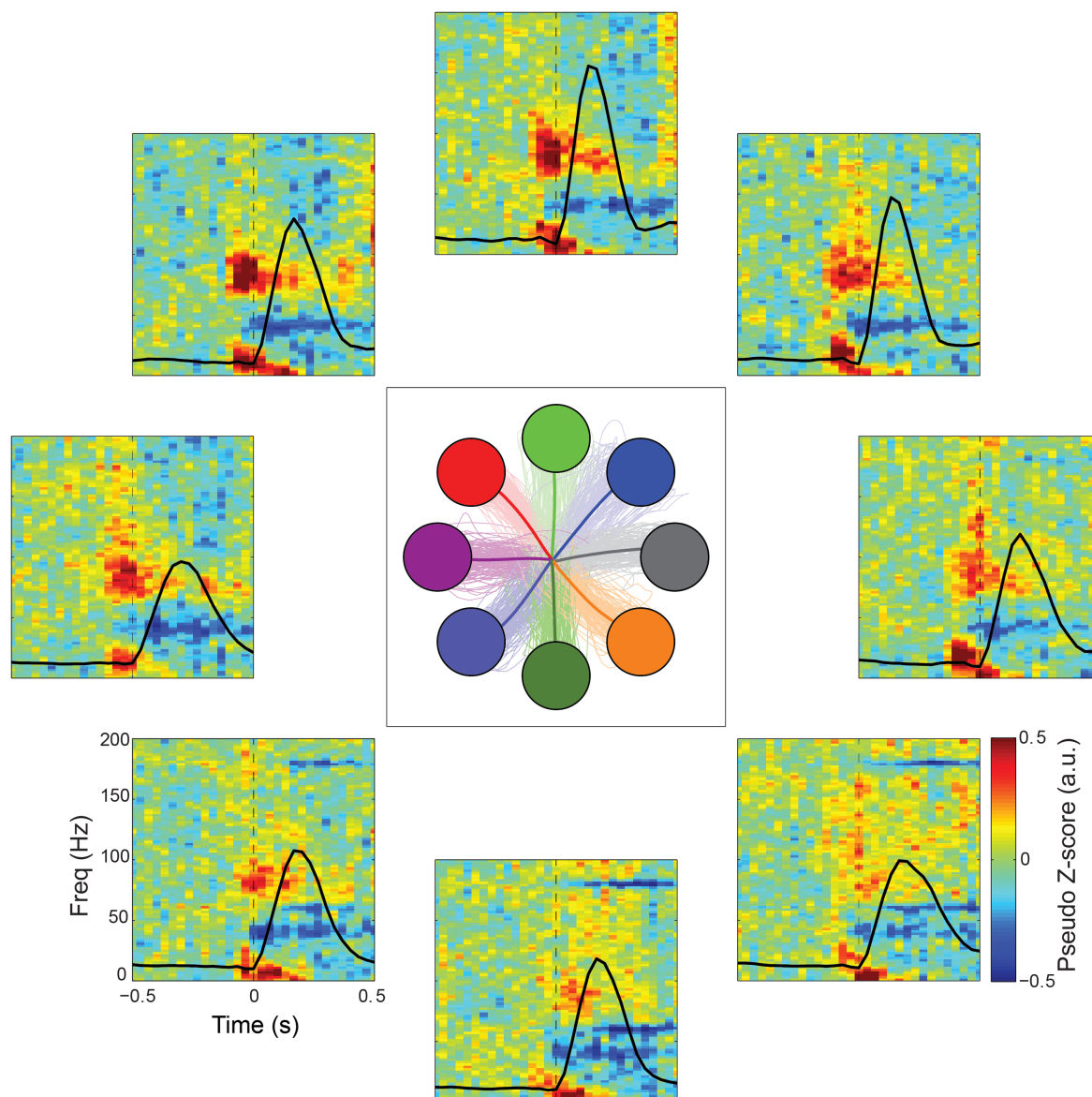
Figure 6. ECoG signal modulation during 8-target center-out reach tasks. Average time–frequency data are shown for a single electrode (e10) for all reach directions. Averaged (thick lines) and individual trajectories (thin lines) for each target are shown in the center panel. Time–frequency data were normalized with respect to the spectral data during a central hold period preceding each trial. Black lines show average speed profiles for each target.

regrown dura at 3 weeks and a 3.1 fold increase at 3 months. Dural thickening of 2 mm 8 weeks after a 2 cm dural incision has also been observed in coonhound dogs; following application of a poly(ethylene) glycol based dural sealant, the healed dura was found to have thickened as much as 4 mm (Preul *et al* 2003). Meningeal cells almost double collagen production following sub-arachnoid hemorrhage in rats (Sajanti *et al* 1999); computational models of collagen I fibrosis following biomaterial implantation corroborate this (Su *et al* 2011). In these experiment-validated models, increasing numbers of fibroblasts at the implant site results in significantly increased collagen deposition. Since the predominating cell type of dura mater is the fibroblast, it is plausible that we might expect pronounced collagen I production following implantation.

Despite the degree of encapsulation, the ECoG grid was extracted from the fibrous tissue with little effort, indicating relatively minor adhesions between the encapsulation and device. This is presumably due to the lack of porosity and surface features on the silicone grid. Previous studies have demonstrated that smooth, non-porous dural substitutes are less susceptible to fibrosis and adhesion formation (Barbolt *et al* 2001, Sayama *et al* 2014).

While we have shown that the foreign body response to chronic ECoG grid implantation can result in grid encapsulation after approximately 22 months, we were unable to determine its exact time course. It is unclear whether the encapsulation was stable, still growing, or perhaps shrinking, at the time of electrode explantation. Subdural ECoG electrodes implanted up to 30 d clinically for epilepsy monitoring

do not exhibit such encapsulation (Fountas and Smith 2007, Van Gompel *et al* 2008, Wong *et al* 2009, Wang *et al* 2013), so it is likely that the subdural implant encapsulation response occurs on the order of months rather than weeks. Meningeal thickening without encapsulation has been observed in micro-ECoG arrays in rats at 6 months post-implant, though no other time-points were assessed (Henle *et al* 2011). In contrast, epidural implant encapsulation has been observed as soon as one month post-implant, with dramatically slower tissue encapsulation observed under an epidural array that had torn the dura mater during implantation (Schendel *et al* 2013, Schendel *et al* 2014). This suggests that there may be different foreign body response mechanisms for implants with different degrees of invasiveness. To our knowledge, there is no study directly comparing implantation depth to explore possible foreign body response mechanisms.

4.2. ECoG recording quality

ECoG electrodes provided recordings of physiological signals for nearly 2 years. Issues with the animal that were unrelated to the ECoG grid determined the termination date of the study, but we believe that signal quality may have persisted past two years. Of the 15 electrodes on the array, only one lost recording capability during the course of our study. Post-explantation, we determined that failure was on account of a faulty wire connecting the Cereport adapter to the neural amplifier. We found that all functional electrodes showed signals that were temporally modulated and spatially tuned during a reaching task.

We conducted extensive BMI control tasks as part of this study. By the time we detected that the animal had developed a strategy of generating an electromyographic artifact (believed to be the result of jaw or face muscle contraction) to control the cursor, we were unable to train him to abandon this strategy. This made it difficult to study the functional properties of ECoG signals during the BMI control sessions. Despite the lack of longitudinal BCI performance data, both impedance and RMS amplitude measurements were relatively stable from day 56 (our earliest time-point measured) to day 562 post-implantation. The stable impedance and RMS amplitude suggest that the encapsulation did not significantly compromise the device functionality. However, future studies using a stereotypical experimental paradigm, such as the center-out task, will likely be able to better characterize changes in ECoG signal properties throughout the entire lifespan of an ECoG implant.

4.3. Implications and future directions

We believe our results have implications for the viability of ECoG for long-term high-resolution brain recording. In addition to its use as a recording modality for BMIs, ECoG has increasingly become a neuroimaging method of choice in a variety of neuroscience fields and non-BMI neural recording and neuromodulation applications. The potential for subdural ECoG grids to remain implanted for extended periods of time without damaging the cortex could facilitate the study of cognitive processes over long timescales. Lack of cortical damage combined with the ease of removal of the ECoG grid from encapsulation tissue may provide the possibility for re-implantation in case of device failure. This is not practical for intracortical electrodes, which typically damage neural tissue upon insertion (Barrese *et al* 2013). While ECoG grid encapsulation presents as a potentially detrimental consequence of implantation, many strategies can and have been pursued to minimize the foreign body response. These include altering the shape of array substrate (Yamakwa *et al* 2010, Schendel *et al* 2013, Schendel *et al* 2014), increasing array flexibility (Yeager *et al* 2008, Rubehn *et al* 2009, Kim *et al* 2010), applying anti-fouling or biomimetic surface treatments (Collier *et al* 2004, Kolarcik *et al* 2012), and releasing anti-inflammatory drugs from the array substrate or electrodes (Norton *et al* 2005, Weaver *et al* 2014). Use of such strategies may help to further increase the stability of long-term ECoG recordings by eliminating changes in recording quality resulting from the foreign body response to subdural ECoG grids.

As the presented work constitutes a case study of long-term grid implantation in a single animal, future studies are required to fully assess the impact of chronically-implanted ECoG electrodes. Nevertheless, our findings of meningeal thickening, encapsulation, and fibrosis echo studies on subdural and epidural implants in rats (Henle *et al* 2011, Schendel *et al* 2013, Schendel *et al* 2014), NHP (Ryapolova-Webb *et al* 2014), as well as in long-term (>1 year) subdural and epidural implants in humans (Nashold and Friedman 1972, Pineda 1978, Saitoh *et al* 2000, Sillay *et al* 2013). There are fewer studies on the health of neural tissue underlying these implants. Additionally, we believe that our results provide an analytical framework for further investigation into the effects of chronic implantation of ECoG electrodes on the health of cortical tissue.

This study is an important first step toward fully assessing the long-term use of chronically implanted ECoG electrode grids. Minimal cortical tissue damage from chronic electrode implantation suggests that ECoG may provide the capability to record physiological signals from the cortex for extended periods of time. Ultimately, this highlights the utility of ECoG as a valuable tool for long-term BMI, clinical, and neuroscientific studies.

Acknowledgments

References

Acharya S, Fifer M S, Benz H L, Crone N E and Thakor N V 2010 Electrocorticographic amplitude predicts finger positions during slow grasping motions of the hand *J. Neural Eng.* **7** 046002

Adeeb N, Mortazavi M M, Tubbs R S and Cohen-Gadol A A 2012 The cranial dura mater: a review of its history, embryology, and anatomy *Child's Nervous Syst.* **28** 827–37

Anderson J M 2001 Biological response to materials *Annu. Rev. Mater. Res.* **31** 81–100

Anderson J M, Rodriguez A and Chang D T 2008 Foreign body reaction to biomaterials *Semin. Immunol.* **20** 86–100

Ashmore R, Endler B, Smalianchuk I, Degenhart A, Hatsopoulos N, Tyler-Kabara E, Batista A and Wang W 2012 Stable online control of an electrocorticographic brain-computer interface using a static decoder *Conf. Proc. IEEE Eng. Med. Biol. Soc.* **2012** 1740–4

Ball T, Schulze-Bonhage A, Aertsen A and Mehring C 2009 Differential representation of arm movement direction in relation to cortical anatomy and function *J. Neural Eng.* **6** 016006

Barbolt T A, Odin M, Léger M, Kangas L, Holste J and Liu S H 2001 Biocompatibility evaluation of dura mater substitutes in an animal model *Neurol. Res.* **23** 813–20

Barrese J C, Rao N, Paroo K, Triebwasser C, Vargas-Irwin C, Franquemont L and Donoghue J P 2013 Failure mode analysis of silicon-based intracortical microelectrode arrays in non-human primates *J. Neural Eng.* **10** 066014

Biran R, Martin D C and Tresco P A 2005 Neuronal cell loss accompanies the brain tissue response to chronically implanted silicon microelectrode arrays *Exp. Neurol.* **195** 115–26

Brodbeck W G, Shive M S, Colton E, Ziats N P and Anderson J M 2002 Interleukin-4 inhibits tumor necrosis factor-alpha-induced and spontaneous apoptosis of biomaterial-adherent macrophages *J. Lab. Clin. Med.* **139** 90–100

Chao Z C, Nagasaka Y and Fujii N 2010 Long-term asynchronous decoding of arm motion using electrocorticographic signals in monkeys *Frontiers Neuroeng.* **3** 3

Chestek C A *et al* 2011 Long-term stability of neural prosthetic control signals from silicon cortical arrays in rhesus macaque motor cortex *J. Neural Eng.* **8** 045005

Chestek C A, Gilja V, Blabe C H, Foster B L, Shenoy K V, Parvizi J and Henderson J M 2013 Hand posture classification using electrocorticography signals in the gamma band over human sensorimotor brain areas *J. Neural Eng.* **10** 026002

Collier T O, Anderson J M, Brodbeck W G, Barber T and Healy K E 2004 Inhibition of macrophage development and foreign body giant cell formation by hydrophilic interpenetrating polymer network *J. Biomed. Mater. Res.* A **69** 644–50

Collinger J L, Wodlinger B, Downey J E, Wang W, Tyler-Kabara E C, Weber D J, McMorland A J, Velliste M, Boninger M L and Schwartz A B 2012 High-performance neuroprosthetic control by an individual with tetraplegia *Lancet* **381** 507–98

Cox G, Kable E, Jones A, Fraser I, Manconi F and Gorrell M D 2003 3-dimensional imaging of collagen using second harmonic generation *J. Struct. Biol.* **141** 53–62

Crone N E, Hao L, Hart J, Boatman D, Lesser R P, Irizarry R and Gordon B 2001 Electrocorticographic gamma activity during word production in spoken and sign language *Neurology* **57** 2045–53

Crone N E, Miglioretti D L, Gordon B, Sieracki J M, Wilson M T, Uematsu S and Lesser R P 1998 Functional mapping of human sensorimotor cortex with electrocorticographic spectral analysis. I. Alpha and beta event-related desynchronization *Brain.* **191**(Pt 12) 2271–99

Degenhart A D, Collinger J L, Vinjamuri R, Kelly J, Tyler-Kabara E C and Wang W 2011a Classification of hand posture from electrocorticographic signals recorded during varying force conditions *Engineering in Medicine and Biology Society, EMBC, 2011 Annual Int. Conf. of the IEEE*

Degenhart A D, Kelly J W, Ashmore R C, Collinger J L, Tyler- Kabara E C, Weber D J and Wang W 2011b Craniux: a LabVIEW-based modular software framework for brain-machine interface research *Comput. Intell. Neurosci.* **2011** 363565

Ding M C, Lo E H and Stanley G B 2008 Sustained focal cortical compression reduces electrically induced seizure threshold *Neuroscience* **154** 551–5

Edwards E, Soltani M, Deouell L Y, Berger M S and Knight R T 2005 High gamma activity in response to deviant auditory stimuli recorded directly from human cortex *J. Neurophysiol.* **94** 4269–80

Eng L F, Ghirnikar R S and Lee Y L 2000 Glial fibrillary acidic protein: GFAP-thirty-one years (1969–2000) *Neurochem. Res.* **25** 1439–51

Fountas K N and Smith J R 2007 Subdural electrode-associated complications: a 20-year experience *Stereotactic Funct. Neurosurg.* **85** 264–72

Freire M A M, Morya E, Faber J, Santos J R, Guimaraes J S, Lemos N A, Sameshima K, Pereira A, Ribeiro S and Nicolelis M A 2011 Comprehensive analysis of tissue preservation and recording quality from chronic multielectrode implants *PLoS One* **6** e27554

Gittins R and Harrison P J 2004 Neuronal density, size and shape in the human anterior cingulate cortex: a comparison of Nissl and NeuN staining *Brain Res. Bull.* **63** 155–60

Griffith G W and Humphrey D R 2006 Long-term gliosis around chronically implanted platinum electrodes in the *Rhesus macaque* motor cortex *Neurosci. Lett.* **406** 81–6

Henle C, Raab M, Cordeiro J G, Doostkam S, Schulze-Bonhage A, Stieglitz T and Rickert J 2011 First long term in vivo study on subdurally implanted micro-ECoG electrodes, manufactured with a novel laser technology *Biomed. Microdevices* **13** 59–68

Hotson G *et al* 2016 Individual finger control of a modular prosthetic limb using high-density electrocorticography in a human subject *J. Neural Eng.* **13** 026017

Jung J, Mainy N, Kahane P, Minotti L, Hoffmann D, Bertrand O and Lachaux J-P 2008 The neural bases of attentive reading *Hum. Brain Mapp.* **29** 1193–206

Kellis S, Miller K, Thomson K, Brown R, House P and Greger B 2010 Decoding spoken words using local field potentials recorded from the cortical surface *J. Neural Eng.* **7** 056007

Kim D H *et al* 2010 Dissolvable films of silk fibroin for ultrathin conformal bio-integrated electronics *Nat. Mater.* **9** 511–7

Kim J J and Gean A D 2011 Imaging for the diagnosis and management of traumatic brain injury *Neurotherapeutics: J. Am. Soc. Exp. NeuroTherapeutics* **8** 39–53

Kolarcik C L, Bourbeau D, Azemi E, Rost E, Zhang L, Lagenaur C F, Weber D J and Cui X T 2012 In vivo effects of L1 coating on inflammation and neuronal health at the electrode/tissue interface in rat dorsal root ganglion and spinal cord *Acta Biomater.* **8** 3561–75

Konsui R, Beynon S B, Johnson S J and Walker F R 2014 Quantitative assessment of microglial morphology and density reveals remarkable consistency in the distribution and morphology of cells within the healthy prefrontal cortex of the rat *J. Neuroinflammation* **11** 182

Kozai T D Y, Vasquez A L, Weaver C L, Kim S-G and Cui X T 2012 In vivo two-photon microscopy reveals immediate microglial reaction to implantation of microelectrode through extension of processes *J. Neural Eng.* **9** 066001

Kubanek J, Miller K J, Ojemann J G, Wolpaw J R and Schalk G 2009 Decoding flexion of individual fingers using electrocorticographic signals in humans *J. Neural Eng.* **6** 066001

Lachaux J-P, George N, Tallon-Baudry C, Martinerie J, Hugueville L, Minotti L, Kahane P and Renault B 2005 The many faces of the gamma band response to complex visual stimuli *NeuroImage* **25** 491–501

Leuthardt E C, Gaona C, Sharma M, Szrama N, Roland J, Freudenberg Z, Solis J, Breshears J and Schalk G 2011 Using the electrocorticographic speech network to control a brain-computer interface in humans *J. Neural Eng.* **8** 036004

Leuthardt E C, Schalk G, Moran D and Ojemann J G 2006 The emerging world of motor neuroprosthetics: a neurosurgical perspective *Neurosurgery* **59** 1–14

Leuthardt E C, Schalk G, Wolpaw J R, Ojemann J G and Moran D W 2004 A brain-computer interface using electrocorticographic signals in humans *J. Neural Eng.* **1** 63–71

Lynn A D, Blakney A K, Kyriakides T R and Bryant S J 2010 Temporal progression of the host response to implanted poly (ethylene glycol)-based hydrogels *J. Biomed. Mater. Res.* A **96** 621–31

Mainy N, Kahane P, Minotti L, Hoffmann D, Bertrand O and Lachaux J-P 2007 Neural correlates of consolidation in working memory *Hum. Brain Mapp.* **28** 183–93

Matelli M, Luppino G and Rizzolatti G 1991 Architecture of superior and mesial area 6 and the adjacent cingulate cortex in the macaque monkey *J. Comparative Neurol.* **311** 445–62

McConnell G C, Rees H D, Levey A I, Gutekunst C-A, Gross R E and Bellamkonda R V 2009 Implanted neural electrodes cause chronic, local inflammation that is correlated with local neurodegeneration *J. Neural Eng.* **6** 056003

Miller K J, Leuthardt E C, Schalk G, Rao R P, Anderson N R, Moran D W, Miller J W and Ojemann J R 2007 Spectral changes in cortical surface potentials during motor movement *J. Neurosci.* **27** 2424–32

Miller K J, Zanos S, Fetz E E, Den Nijs M and Ojemann J G 2009 decoupling the cortical power spectrum reveals real-time representation of individual finger movements in humans *J. Neurosci.* **29** 3132–7

Moran D 2010 Evolution of brain-computer interface: action potentials, local field potentials and electrocorticograms *Curr. Opin. Neurobiol.* **20** 741–5

Morrell M J and RNS System in Epilepsy Study Group 2011 Responsive cortical stimulation for the treatment of medically intractable partial epilepsy *Neurology* **77** 1295–304

Nakanishi Y, Yanagisawa T, Shin D, Fukuma R, Chen C, Kambara H, Yoshimura N, Hirata M, Yoshimine T and Koike Y 2013 Prediction of three-dimensional arm trajectories based on ECoG signals recorded from human sensorimotor *Cortex. PLoS One* **8** e72085

Nashold B S and Friedman H 1972 Dorsal column stimulation for control of pain: preliminary report on 30 patients *J. Neurosurg.* **36** 490–7

Nimmerjahn A, Kirchhoff F and Helmchen F 2005 Resting microglial cells are highly dynamic surveillants of brain parenchyma in vivo *Science* **308** 1314–8

Norton L W, Tegnell E, Toporek S S and Reichert W M 2005 In vitro characterization of vascular endothelial growth factor and

dexamethasone releasing hydrogels for implantable probe coatings *Biomaterials* **26** 3285–97

Nunamaker E A and Kipke D R 2010 An alginate hydrogel dura mater replacement for use with intracortical electrodes *J. Biomed. Mater. Res.* **95** 421–9

Pei X, Barbour D L, Leuthardt E C and Schalk G 2011 Decoding vowels and consonants in spoken and imagined words using electrocorticographic signals in humans *J. Neural Eng.* **8** 046028

Peters A and Sethares S 2002 The effects of age on the cells in layer 1 of primate cerebral cortex *Cerebral Cortex* **12** 27–36

Pineda A 1978 Complications of dorsal column stimulation *J. Neurosurg.* **48** 64–8

Pistohl T, Ball T, Schulze-Bonhage A, Aertsen A and Mehring C 2008 Prediction of arm movement trajectories from ECoG-recordings in humans *J. Neurosci. Methods* **167** 105–14

Polikov V S, Tresco P A and Reichert W M 2005 Response of brain tissue to chronically implanted neural electrodes *J. Neurosci. Methods* **148** 1–18

Preibisch S, Saalfeld S and Tomancak P 2009 Globally optimal stitching of tiled 3D microscopic image acquisitions *Bioinformatics* **25** 1463–5

Preul M C, Bichard W D and Spetzler R F 2003 Toward optimal tissue sealants for neurosurgery: use of a novel hydrogel sealant in a canine durotomy repair model *Neurosurgery* **53** 1189–98

Ray S, Niebur E, Hsiao S S, Sinai A and Crone N E 2008 High-frequency gamma activity (80–150 Hz) is increased in human cortex during selective attention *Clin. Neurophysiol.: Official J. Int. Fed. Clin. Neurophysiol.* **119** 116–33

Roth T L, Nayak D, Atanasijevic T, Koretsky A P, Latour L L and McGavern D B 2014 Transcranial amelioration of inflammation and cell death after brain injury *Nature* **505** 223–8

Rubehn B, Bosman C, Oostenveld R, Fries P and Stieglitz T 2009 A MEMS-based flexible multichannel ECoG-electrode array *J. Neural Eng.* **6** 036003

Ryapolova-Webb E, Afshar P, Stanslaski S, Denison T, de Hemptinne C, Bankiewicz K and Starr P A 2014 Chronic cortical and electromyographic recordings from a fully implantable device: preclinical experience in a nonhuman primate *J. Neural Eng.* **11** 016009

Saitoh Y, Shibata M, Hirano S-I, Hirata M, Mashimo T and Yoshimine T 2000 Motor cortex stimulation for central and peripheral deafferentation pain: report of eight cases *J. Neurosurg.* **92** 150–5

Sajanti J, Bjorkstrand A-S, Finnila S, Heikkinen E, Peltonen J and Majamaa K 1999 Increase of collagen synthesis and deposition in the arachnoid and the dura following subarachnoid hemorrhage in the rat *Biochim. Biophys. Acta* **1454** 209–16

Sanders J E, Stiles C E and Hayes C L 2000 Tissue response to single-polymer fibers of varying diameters: evaluation of fibrous encapsulation and macrophage density *J. Biomed. Mater. Res.* **52** 231–7

Sayama C M, Sorour M and Schmidt R H 2014 Dural adhesion to porous cranioplastic implant: a potential safety concern *Surg. Neurol. Int.* **5** 19

Schalk G, Kubanek J, Miller K J, Anderson N R, Leuthardt E C, Ojeymann J G, Limbrick D, Moran D, Gerhardt L A and Wolpaw J R 2007 Decoding two-dimensional movement trajectories using electrocortical movement trajectories using electrocorticographic signals in humans *J. Neural Eng.* **4** 264–75

Schalk G and Lethardt E C 2011 Brain-computer interfaces using electrocorticographic signals *IEEE Rev. Biomed. Eng.* **4** 140–54

Schalk G, Miller K J, Anderson N R, Wilson J A, Smyth M D, Ojemann J G, Moran D W, Wolpaw J R and Leuthardt E C

2008 Two-dimensional movement control using electrocorticographic signals in humans *J. Neural Eng.* **5** 75–84

Schendel A A *et al* 2014 The effect of micro-ECoG substrate footprint on the meningeal tissue response *J. Neural Eng.* **11** 046011

Schendel A A, Thongpang S, Brodnick S K, Richner T J, Lindevig B D B, Krugner-Higby L and Williams J C 2013 A cranial window imaging method for monitoring vascular growth around chronically implanted micro-ECoG devices *J. Neurosci. Methods* **218** 121–30

Schwartz A B 2004 Cortical neural prosthetics *Annu. Rev. Neurosci.* **27** 487–507

Schwartz A B, Cui X T, Weber D J and Moran D W 2006 Brain-controlled interfaces: movement restoration with neural prosthetics *Neuron* **52** 205–20

Shimoda K, Nagasaka Y, Chao Z C and Fujii N 2012 Decoding continuous three-dimensional hand trajectories from epidural electrocorticographic signals in Japanese macaques *J. Neural Eng.* **9** 036015

Sillay K A, Rutecki P, Cicora K, Worrell G, Drazkowski J, Shih J J, Sharan A D, Morrell M J, Williams J and Wingeier B 2013 Long-term measurement of impedance in chornically implanted depth and subdural electrodes during responsive neurostimulation in humans *Brain Stimulation* **6** 718–26

Simeral J D, Kim S-P, Black M J, Donoghue J P and Hochberg L R 2011 Neural control of cursor trajectory and click by a human with tetraplegia 1000 days after implant of an intracortical microelectrode array *J. Neural Eng.* **8** 025027

Stence N, Waite M and Dailey M E 2001 Dynamics of microglial activation: a confocal time-lapse analysis in hippocampal slices *Glia* **33** 256–66

Strupler M, Pena A M, Hernest M, Tharaux P L, Martin J L, Beaurepaire E and Schanne-Klein M C 2007 Second harmonic imaging and scoring of collagen in fibrotic tissues *Opt. Express* **15** 4054–65

Su J, Todorov M, Gonzales H P, Perkins L, Kojouharov H, Weng H and Tang L 2011 A predictive tool for foreign body fibrotic reactions using 2-dimensional computational model *Open Access Bioinf.* **3** 19–35

Tallon-Baudry C, Bertrand O, Hénaff M-A, Isnard J and Fischer C 2005 Attention modulates gamma-band oscillations differently in the human lateral occipital cortex and fusiform gyrus *Cerebral Cortex* **15** 654–62

Trautner P, Rosburg T, Dietl T, Fell J, Korzyukov O A, Kurthen M, Schaller C, Elger C E and Boutros N N 2006 Sensory gating of auditory evoked and induced gamma band activity in intracranial recordings *NeuroImage* **32** 790–8

Van Gompel J J, Worrell G A, Bell M L, Patrick T A, Cascino G D, Raffel C, Marsh W R and Meyer F B 2008 Intracranial

electroencephalography with subdural grid electrodes: techniques, complications, and outcomes *Neurosurgery* **63** 498–505

Vela J M, Dalmau I, Gonzalez B and Castellano B 1995 Morphology and distribution of microglial cells in the young and adult mouse cerebellum *J. Comparative Neurol.* **361** 602–16

Wang W *et al* 2009 Human motor cortical activity recorded with Micro-ECoG electrodes, during individual finger movements *Conf. Proc.: Annual Int. Conf. of the IEEE Engineering in Medicine and Biology Society IEEE Engineering in Medicine and Biology Society Conf.* vol 2009 pp 586–9

Wang W *et al* 2013 An electrocorticographic brain interface in an individual with tetraplegia *PLoS One* **8** e55344

Wang W, Degenhart A D, Sudre G P, Pomerleau D and Tyler-Kabara E C 2011 Decoding semantic information from human electrocorticographic (ECoG) signals *Engineering in Medicine and Biology Society,EMBC, 2011 Annual Int. Conf. of the IEEE* vol 2011 pp 6294–8

Wang Y, Papadimitrakopoulos F and Burgess D J 2013 Polymeric 'smart' coatings prevent foreign body response to implantable biosensors *J. Control. Release* **169** 341–7

Weaver C L, LaRosa J M, Luo X and Cui X T 2014 Electrically controlled drug delivery from graphene oxide nanocomposite films *ACS Nano* **8** 1834–43

Wilson J A, Felton E A, Garell P C, Schalk G and Williams J C 2006 ECoG factors underlying multimodal control of a brain-computer interface *IEEE Transactions on Neural Systems and Rehabilitation Engineering: a Publication of the IEEE Engineering in Medicine and Biology Society* **vol 14** pp 246–50

Wolpaw J R, Birbaumer N, McFarland D J, Pfurtscheller G and Vaughan T M 2002 Brain-computer interfaces for communication and control *Clin. Neurophysiol.: Official J. Int. Fed. Clin. Neurophysiol.* **113** 767–91

Wong C H, Birkett J, Byth K, Dexter M, Somerville E, Gill D, Chaseling R, Fearnside M and Bleasel A 2009 Risk factors for complications during intracranial electrode recording in presurgical evaluation of drug resistant partial epilepsy *Acta Neurochirurgica* **151** 37–50

Yamakawa T, Yamakwa T, Aou S, Ishizuka S, Suzuki M and Fujii M 2010 Subdural electrode array manipulated by a shape memory allow guidewire for minimally-invasive electrocorticogram recording *World Automation Congress*

Yanagisawa T, Hirata M, Saitoh Y, Kishima H, Matsushita K, Goto T, Fukuma R, Yokoi H, Kamitani Y and Yoshimine T 2012 Electrocorticographic control of a prosthetic arm in paralyzed patients *Ann. Neurol.* **71** 353–61

Yeager J D, Phillips D J, Rector D M and Bahr D F 2008 Characterization of flexible ECoG electrode arrays for chronic recording in awake rats *J. Neurosci. Methods* **173** 279–85